Second harmonic generation from an antiferromagnetic film in one-dimensional photonic crystals

Sheng Zhou,[1,2] Hua Li,[2] Shu-Fang Fu,[2] and Xuan-Zhang Wang[2,*]
[1]*School of Electric Engineering, Harbin University of Science and Technology, Harbin 150080, China*
[2]*Provincial Key Laboratory for Advanced Functional Material and Excited States Processes, School of Physics and Electronic Engineering, Harbin Normal University, Harbin 150025, China*
(Received 15 May 2009; revised manuscript received 9 October 2009; published 10 November 2009)

We calculate the second harmonic generation (SHG) from an antiferromagnetic film (AFF) embedded in a one-dimension photonic crystal. The electromagnetic wave localization in the AFF leads to a giant enhancement of the SHG. The numerical results based on three typical structures show that the highest power of SH outputs reaches several hundred times that of a single AFF for the same incident power. The SH outputs depend sensitively on the structural geometry and symmetry, and the best structure and the best layer-thickness matching for it are found. The SHG nonreciprocity is very obvious; i.e., if the direction of incident radiation is reversed, the SH output powers can be changed by several dozens times. Three narrow and obvious SHG bands are found.

DOI: 10.1103/PhysRevB.80.205409 PACS number(s): 78.66.−w, 42.65.Ky, 42.70.Qs, 75.50.Ee

I. INTRODUCTION

Since Almeida, Mills and Kahn *et al.* first discussed the nonlinearity of antiferromagnetic (AF) films and superlattices,[1,2] the AF second-order and third-order effects have been paid a great deal of attention to.[3–7] The resonant frequencies of typical AF materials are distributed over the millimeter and far-infrared ranges,[8] so their nonlinearity is of practical interest in these ranges. The second harmonic generation (SHG) technique is widely used as one method of frequency conversion,[9] and this method is a common tool to produce new light sources at frequencies where no laser is available. Generally speaking, the AF nonlinearity is weak, but it may be very interesting since scientists are attempting to develop the THz technology for the future communication and detection. In order to obtain observable nonlinear properties of a single AF film (AFF) or an AF superlattice, one needs very strong incident electromagnetic waves, or strong lights[3,4] to irradiate it. It means that there are some serious difficulties on the present technical level. Therefore, it is a very interesting subject to look for a method of enhancing the SHG at a proper incident power. In our previous paper,[5] one method was presented to enlarge the SH outputs, where an AFF was sandwiched between two different dielectrics. Numerical results show that the highest SH output obtained comes to at least a hundred times that of a single AFF. Notably, the nonlinearity mentioned above results from the magnetic dipole-dipole interaction between electromagnetic waves and AF dynamic magnetizations. Recently other papers were also offered to studying the SHG of antiferromagnets,[10–13] but the AF nonlinearity in those papers is attributed to the combined contributions of the magnetic-dipole and electric-dipole transitions, and is available in the near-infrared and visible-light regions. They concluded that the nonlinearity can be used to determine the magnetic structure of the AF media, especially surface and domain structures.

Photonic crystals (PCs) have two essential and useful characteristics, or the existence of photonic band gaps and localization modes.[14–16] When some AFFs as defect layers are introduced into a one-dimension PC, the defect modes may appear in the band gaps. Thus electromagnetic radiations corresponding to the defect modes can enter the PC and be localized in the AFFs. This localization effect has been applied to the SHG from a traditional nonlinear film embedded in one-dimension photonic crystals,[17–20] where a giant enhancement of the SHG was found. Therefore, in the situation of electromagnetic localization, as long as the incident-wave frequency is near to either of the two AF resonant frequencies, the nonlinearity can be greatly enhanced. In addition, magnetic photonic crystals also have been paid a great deal of attention to,[21,22] where the nonlinearity also is an important subject.[23] The propagation nonreciprocity of electromagnetic wave and the giant Faraday effect[24–26] were found. We present another method in this paper to enlarge the SHG of an AFF.

II. THEORETICAL FORMALISM

We apply three typical structures with different symmetries, as shown in Fig. 1. The first structure contains a PC with even number of dielectric bilayers and an AFF as the central layer, shown in Fig. 1(a). The second consists of a PC with odd number of dielectric bilayers and an AFF as the central layer, illustrated in Fig. 1(b). The last contains even number of the bilayers and AFF, but is structurally symmetrical, as shown in Fig. 1(c). We use such a coordinate system with the y axis normal to layers in the PC. The external magnetic field and the AF anisotropic field both are pointed along the z axis. The x-y plane is used as the plane of incidence. I, R, and T indicate the incident, reflection and transmission waves, respectively. θ and θ' are the angles of incidence and transmission. The SH waves R_s and T_s radiated from the structures propagate in the directions shown by angles θ_s and θ_s'. The thicknesses of dielectric layers and AFF are d_1, d_2, and d_a, where subscripts 1, 2, and a represent two kinds of dielectric layers and the AFF, and their dielec-

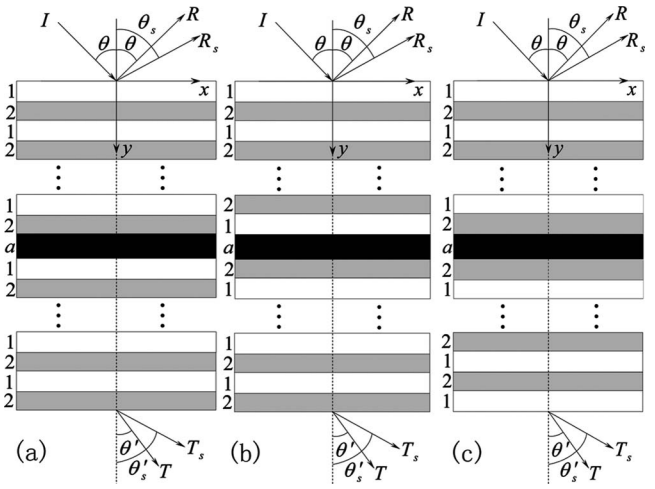

FIG. 1. Structures and geometries: I, R, and T are the incident, reflective and transmission waves with incident angle θ and transmission angle θ', R_s, and T_s indicate the outputted SH waves with direction angles θ_s and θ'_s. The x-y plane is considered as the incident plane, and the external magnetic field $\vec{H}_0$ and the AF anisotropy field $\vec{H}_a$ both are pointed along the z axis.

tric constants ε_1, ε_2, and ε_a, respectively. The magnetic permeability of nonmagnetic media is taken as $\mu_0=1$. The derivations of linear and SH magnetic susceptibilities of an uniaxial antiferromagnet are put in the Appendix, where we describe the AF structure and relevant physical quantities. We shall directly use the results obtained there. The AF linear magnetic permeability is $\vec{\vec{\mu}}_a=1+\vec{\vec{\chi}}_a$ and the nonzero elements of the susceptibility $\vec{\vec{\chi}}_a$ are

$$\chi_{xx}=\chi_{yy}=\chi_1=\omega'_a\omega_m\{1/[\omega'^2_r-(\omega-\omega_0)^2] + 1/[\omega'^2_r-(\omega+\omega_0)^2], \quad (1a)$$

$$\chi_{xy}=-\chi_{yx}=i\chi_2=i\omega'_a\omega_m\{1/[\omega'^2_r-(\omega-\omega_0)^2] - 1/[\omega'^2_r-(\omega+\omega_0)^2], \quad (1b)$$

The SH-susceptibility elements to be applied are

$$\chi^{(2)}_{zxx}=\chi^{(2)}_{zyy}=\frac{2\omega_m^2\omega_0\omega'_a}{M_0[\omega'^2_r-(\omega-\omega_0)^2][\omega'^2_r-(\omega+\omega_0)^2]}, \quad (2)$$

where the special frequencies ω_0, ω_m, ω_a and ω_e are related to the external field (H_0), sublattice magnetization (M_0), anisotropy and exchange fields in the AFF, respectively. $\omega'^2_r=\omega'_a(2\omega_e+\omega'_a)$ with $\omega'_a=\omega_a+i\tau\omega$ (τ is the damping constant). The relevant SH magnetization is[5]

$$m_z^{(2)}(\omega_s)=\chi^{(2)}_{zxx}(H_xH_x+H_yH_y), \quad (3)$$

with $\omega_s=2\omega$. $\vec{H}$ is the magnetic field of a pumping wave with frequency ω.

Two sorts of electromagnetic waves should be mentioned. One is known as the fundamental-frequency waves with frequency ω, called the ω-waves. The ω-wave in the AFF is directly named the pumping wave. The other means electromagnetic waves with frequency ω_s, called the SH waves. The nonmagnetic media used here may be slightly nonlinear and their electric polarization may respond nonlinearly to the electric-field component of an electromagnetic wave, but we are interested in only the magnetic SHG from the AF, so this nonlinearity is assumed to be secondary and ignored. Thus the mathematic process will be simplified. We assume that: (a) the AFF is of nonlinearity and the other media are linear; (b) the energy-conversion efficiency is so low that the deletion of the pumping wave can be neglected. In consequence, solving the pumping wave is a linear problem. For these multilayered structures, the transfer-matrix method is available and it has been widely applied to one-dimension PCs or superlattices.[4,27]

A. Solving the pumping wave in the AFF

Any plane electromagnetic wave of incidence can be decomposed into a TM wave with its magnetic field normal to the incident plane and a TE wave with its electric field normal to the plane. However, the TM wave does not couple with the magnetization in the AFF, so it will not induce any magnetic SH waves in the AFF along, without the TE wave. Therefore, for simplicity, we suppose that all the ω waves are of TE wave. The wave solution in various spaces can be shown by

$$E_z=\exp(ik_xx-i\omega t)\times\begin{cases} I_0\exp(ik_0y)+R_0\exp(-ik_0y), & \text{(in the above space)} \\ A_j\exp(ik_jy)+B_j\exp(-ik_jy), & \text{(in the } j \text{ layer)} \\ T_0\exp(ik_0y), & \text{(in the below space)} \end{cases} \quad (4)$$

where $j=1$, 2, or a. The wave-number components $k_0=[(\omega/c)^2-k_x^2]^{1/2}$, $k_1=[\varepsilon_1(\omega/c)^2-k_x^2]^{1/2}$, $k_2=[\varepsilon_2(\omega/c)^2-k_x^2]^{1/2}$ and $k_a=[\varepsilon_a\mu_v(\omega/c)^2-k_x^2]^{1/2}$ with $k_x=(\omega/c)\sin\theta$ and the AF effective permeability $\mu_v=(\mu_{xx}^2+\mu_{xy}^2)/\mu_{xx}$. The capital characters on the right side of Eq. (4) represent the wave amplitudes in different spaces, where I_0 and R_0 as well as T_0 are related to the incident, reflection and transmission waves, respectively. The wave magnetic field can be derived from $\nabla\times\vec{E}=i\omega\mu_0\vec{H}$ (μ_0 is the vacuum magnetic permeability) in nonmagnetic media and $\nabla\times\vec{E}=i\omega\mu_0\vec{\vec{\mu}}\cdot\vec{H}$ in the AFF. Because the boundary conditions of E_z and H_x continuous at interfaces will be used, the x component of $\vec{H}$ is presented in different media,

$$H_x = \frac{\exp(ik_x x - i\omega t)}{\omega\mu_0} \begin{cases} k_0[I_0 \exp(ik_0 y) - R_0 \exp(-ik_0 y)] \\ k_j[A_j \exp(ik_j y) - B_j \exp(-ik_j y)] \\ (k_a/\mu_v)[(1+\delta)A_a \exp(ik_a y) + (1-\delta)B_a \exp(-ik_a y)] \\ k_0 T_0 \exp(ik_0 y) \end{cases}, \tag{5a}$$

with $\delta = ik_x\chi_2/(\mu_{xx}k_a)$. Although we do not apply the y component of $\vec{H}$ under the boundary conditions, this component in the AFF will be employed to determine the SH magnetization and we find

$$H_y = \frac{k_x \exp(ik_x x - i\omega t)}{\omega\mu_0\mu_v}[(\delta' - 1)A_a \exp(ik_a y) - (\delta' + 1)B_a \exp(-ik_a y)] \tag{5b}$$

with $\delta' = i\chi_2 k_a/(\mu_{xx}k_x)$.

From the boundary conditions, we can find the relation between wave amplitudes in any pair of adjacent media. The amplitude relation at the surface is

$$\begin{pmatrix} I_0 \\ R_0 \end{pmatrix} = T_{t1} \begin{pmatrix} A_1 \\ B_1 \end{pmatrix} \tag{6a}$$

with the matrix

$$T_{t1} = \frac{1}{2k_0} \begin{pmatrix} k_0 + k_1 & k_0 - k_1 \\ k_0 - k_1 & k_0 + k_1 \end{pmatrix}, \tag{6b}$$

The relation between the amplitudes in adjacent dielectric layers 1 and 2 is shown as

$$\begin{pmatrix} A_j \\ B_j \end{pmatrix} = T_{ji} \begin{pmatrix} A_i \\ B_i \end{pmatrix} \quad i,j = 1 \text{ or } 2, \text{ but } i \neq j \tag{7a}$$

with the matrix

$$T_{ji} = \frac{1}{2k_j} \begin{pmatrix} (k_j + k_i)\exp(-ik_j d_j) & (k_j - k_i)\exp(-ik_j d_j) \\ (k_j - k_i)\exp(ik_j d_j) & (k_j + k_i)\exp(ik_j d_j) \end{pmatrix}. \tag{7b}$$

The amplitudes in the dielectric layer j above and adjacent to the AFF and those in the AFF are conjoined by

$$\begin{pmatrix} A_j \\ B_j \end{pmatrix} = T_{ja} \begin{pmatrix} A_a \\ B_a \end{pmatrix} \tag{8a}$$

where

$$T_{ja} = \frac{1}{2} \begin{pmatrix} (1 + \delta_j^+)\exp(-ik_j d_j) & (1 - \delta_j^-)\exp(-ik_j d_j) \\ (1 - \delta_j^+)\exp(ik_j d_j) & (1 + \delta_j^-)\exp(ik_j d_j) \end{pmatrix}, \tag{8b}$$

with $\delta_j^{\pm} = (k_a \pm k_x\mu_{xy}/\mu_{xx})/(\mu_v k_j)$.

The amplitudes in the AFF and those in the layer below and adjacent to the AFF are conjoined by

$$\begin{pmatrix} A_a \\ B_a \end{pmatrix} = T_{aj} \begin{pmatrix} A_j \\ B_j \end{pmatrix}, \tag{9a}$$

where

$$T_{aj} = \frac{\mu_v k_j}{2k_a} \begin{pmatrix} (\delta_j^- + 1)\exp(-ik_a d_a) & (\delta_j^- - 1)\exp(-ik_a d_a) \\ (\delta_j^+ - 1)\exp(ik_a d_a) & (\delta_j^+ + 1)\exp(ik_a d_a) \end{pmatrix}, \tag{9b}$$

Finally, we find the relation at the bottom surface to be

$$\begin{pmatrix} A_j \\ B_j \end{pmatrix} = T_{jb} \begin{pmatrix} T_0 \\ T_0 \end{pmatrix}, \tag{10a}$$

with

$$T_{jb} = \frac{1}{2k_j} \begin{pmatrix} (k_j + k_0)\exp(-ik_j d_j) & 0 \\ 0 & (k_j - k_0)\exp(ik_j d_j) \end{pmatrix}. \tag{10b}$$

Thus we obtain the matrix equation satisfied by the reflection, transmission and incident amplitudes

$$\begin{pmatrix} I_0 \\ R_0 \end{pmatrix} = \prod \begin{pmatrix} T_0 \\ T_0 \end{pmatrix}, \tag{11}$$

where the matrix Π depends on the number of dielectric bilayers and the structure symmetry. For the first structure, it is

$$\prod = T_{t1}(T_{12}T_{21})^{N/2-1}T_{12}T_{2a}T_{a1}(T_{12}T_{21})^{N/2-1}T_{12}T_{2b}, \tag{12}$$

where N is the number of bilayers, but for the second structure it becomes

$$\prod = T_{t1}(T_{12}T_{21})^{(N-1)/2}T_{1a}T_{a2}(T_{21}T_{12})^{(N-1)/2}T_{2b}. \tag{13}$$

For the last one, the matrix should be

$$\prod = T_{t1}(T_{12}T_{21})^{N/2-1}T_{12}T_{2a}T_{a2}(T_{21}T_{12})^{N/2-1}T_{21}T_{1b}. \tag{14}$$

From Eq. (11), one can calculate numerically the transmission and reflection amplitudes.

Subsequently we describe how to solve pumping amplitudes. We find from Eqs. (11)–(14) that pumping amplitudes A_a and B_a satisfy the equation

$$\begin{pmatrix} I_0 \\ R_0 \end{pmatrix} = \prod' \begin{pmatrix} A_a \\ B_a \end{pmatrix}, \tag{15}$$

in which the matrix is indicated by

$$\prod' = T_{t1}(T_{12}T_{21})^{(N/2-1)}T_{12}T_{2a}, \tag{16a}$$

for the first and third structures, as well as

$$\prod' = T_{t1}(T_{12}T_{21})^{(N-1)/2}T_{1a}, \tag{16b}$$

for the second structure. As a result, so long as we obtain the reflective amplitude R_0 from Eq. (11) the pumping amplitudes can be solved from Eq. (15).

B. Deriving the SH outputs

The magnetically optical nonlinearity is different from the ordinary optical nonlinearity. The magnetic optical nonlinearity in magnetic media results from the nonlinear response of dynamical magnetization to the magnetic field $\vec{H}$ of electromagnetic waves,[3–7]

$$\vec{m} = \vec{\chi}^{(1)} \cdot \vec{H} + \vec{\chi}^{(2)}:\vec{H}\vec{H} + \vec{\chi}^{(3)}:\vec{H}\vec{H}\vec{H} + \cdots. \tag{17}$$

We find from the Appendix that the SH magnetization has only one component for a TE pumping wave, component z, so there is only one inhomogeneous equation and the equation's source is directly proportional to the z component,[5]

$$-\left(\frac{\partial^2}{\partial x^2} + \frac{\partial^2}{\partial y^2}\right)H_{sz}(\omega_s) - \varepsilon_a(\omega_s/c)^2 H_{sz}(\omega_s) = \varepsilon_a(\omega_s/c)^2 m_z^{(2)}(\omega_s), \tag{18}$$

where $m_z^{(2)}(\omega_s)$ is shown by Eq. (3) and the magnetic field in this magnetization is just the pumping field determined in Sec. II A. It is evident that the SH wave is a TM wave and does not couple with the magnetization in the AFF. The SH wave in the AFF is excited by the pumping wave induced by the incident wave. Let

$$\vec{H}_s(\omega_s) = \hat{e}_z\{[A_{sa}\exp(ik_{sa}y) + B_{sa}\exp(-ik_{sa}y)]\exp(ik_{sx}x) + [N_1\exp(2ik_a y) + N_2\exp(-2ik_a y) + N_3]\exp(2ik_x x)\}\exp(-i\omega_s t). \tag{19}$$

We find from Eq. (18) that $k_{sa}=[\varepsilon_a(\omega_s/c)^2 - k_{sx}^2]^{1/2}$ and the nonlinear coefficients are

$$N_1 = \frac{\varepsilon_0\chi_{zxx}^{(2)}A_a^2}{\mu_0(\mu_\nu - 1)(\omega\mu_\nu/c)^2}[k_a^2(1+\delta)^2 + k_x^2(1-\delta')^2], \tag{20a}$$

$$N_2 = \frac{\varepsilon_0\chi_{zxx}^{(2)}B_a^2}{\mu_0(\mu_\nu - 1)(\omega\mu_\nu/c)^2}[k_a^2(1-\delta)^2 + k_x^2(1+\delta')^2], \tag{20b}$$

$$N_3 = \frac{8\varepsilon_0\varepsilon_a\chi_{zxx}^{(2)}A_aB_a}{\mu_0 k_{sa}^2\mu_v^2}[k_a^2(1+\delta)(1-\delta) + k_x^2(\delta'-1)(1+\delta')], \tag{20c}$$

with ε_0 the vacuum dielectric constant. The SH wave in nonmagnetic media also is a TM wave, so it is written as

$$H_{sz} = \exp(ik_{sx}x - i\omega_s t)\begin{cases} R_s\exp(-ik_{s0}y) \\ [A_{sj}\exp(ik_{sj}y) + B_{sj}\exp(-ik_{sj}y)] \\ T_s\exp(ik_{s0}y) \end{cases}, \tag{21}$$

j indicates one of dielectric layers. The SH waves radiating from the structures are called the SH outputs with the magnetic amplitudes R_s and T_s. In terms of the phase-match condition, $k_{sx}=2k_x$, the y components of wave number are $k_{s0}=[(\omega_s/c)^2 - k_{sx}^2]^{1/2}=2k_0$ and $k_{sj}=[\varepsilon_j(2\omega/c)^2 - k_{sx}^2]^{1/2}=2k_j$ in the above and below spaces and dielectric layers. As a result, the SH output above the structures propagates in the direction of the reflective wave and the below moves along that of the transmission wave, or $\theta_s=-\theta$ and $\theta_s'=\theta'$. In order to find the SH outputs, we are going to apply the transfer-matrix method again. From $-i\omega_s\varepsilon_0\varepsilon_i\vec{E}_s=\nabla\times\vec{H}_s$, the x component of the SH electric field in the nonmagnetic media is found to be

$$E_{sx} = \frac{\exp(ik_s x - i\omega_s t)}{\omega_s\varepsilon_0} \times \begin{cases} -R_s k_{s0}\exp(-ik_{s0}y) \\ (k_{sj}/\varepsilon_j)[(A_{sj}\exp(ik_{sj}y) - B_{sj}\exp(-ik_{sj}y)] \\ T_s k_{s0}\exp(ik_{s0}y) \end{cases}, \tag{22a}$$

but that in the AFF is found to be

$$E_{sx} = -\frac{\exp(ik_{sx}x - i\omega_s t)}{\omega_s\varepsilon_0\varepsilon_a}\{k_{sa}[(A_{sa}\exp(ik_{sa}y) - B_{sa} \times\exp(-ik_{sa}y)] + 2k_a[N_1\exp(2ik_a y) - N_2\exp(-2ik_a y)]. \tag{22b}$$

By a process similar to that described in Sec. II A, we can find the SH outputs. According to the boundary conditions of the field components H_{sz} and E_{sx} continuous at the interface between two adjacent media, we first see the matrix equation between the SH amplitudes in the AFF and the adjacent layer above the AFF

$$\begin{pmatrix} A_{sj} \\ B_{sj} \end{pmatrix} = M_{ja}\begin{pmatrix} A_{sa} \\ B_{sa} \end{pmatrix} + \Gamma_1, \tag{23}$$

where

$$M_{ja} = \frac{1}{2}\begin{pmatrix} (1+\Delta_{ja})\exp(-ik_{sj}d_j) & (1-\Delta_{ja})\exp(-ik_{sj}d_j) \\ (1-\Delta_{ja})\exp(ik_{sj}d_j) & (1+\Delta_{ja})\exp(ik_{sj}d_j) \end{pmatrix}, \tag{24a}$$

$$\Gamma_1 = \frac{1}{2}\begin{pmatrix} [(1+\Delta_{ja}')N_1 + (1-\Delta_{ja}')N_2 + N_3]\exp(-ik_{sj}d_j) \\ [(1-\Delta_{ja}')N_1 + (1-\Delta_{ja}')N_2 + N_3]\exp(ik_{sj}d_j) \end{pmatrix}, \tag{24b}$$

with $\Delta_{ja}=\varepsilon_j k_{sa}/\varepsilon_a k_{sj}$ and $\Delta_{ja}'=2\varepsilon_j k_a/\varepsilon_a k_{sj}$. In addition, the relation between the SH amplitudes in the AFF and adjacent layer below the AFF

$$\begin{pmatrix} A_{sa} \\ B_{sa} \end{pmatrix} = T_{aj}\begin{pmatrix} A_{sj} \\ B_{sj} \end{pmatrix} + \Gamma_2, \tag{25}$$

$$M_{ja} = \frac{1}{2\Delta_{ja}} \begin{pmatrix} (\Delta_{ja}+1)\exp(-ik_{sa}d_a) & (\Delta_{ja}-1)\exp(-ik_{sa}d_a) \\ (\Delta_{ja}-1)\exp(ik_{sa}d_a) & (\Delta_{ja}+1)\exp(ik_{sa}d_a) \end{pmatrix}, \tag{26a}$$

$$\Gamma_2 = -\frac{1}{2k_{sa}} \begin{pmatrix} [(k_{sa}+2k_a)N_1 \exp(2ik_a d_a) + (k_{sa}-2k_a)N_2 \exp(-2ik_a d_a) + N_3]\exp(-ik_{sa}d_a) \\ [(k_{sa}-2k_a)N_1 \exp(2ik_a d_a) + (k_{sa}+2k_a)N_2 \exp(-2ik_a d_a) + N_3]\exp(ik_{sa}d_a) \end{pmatrix}. \tag{26b}$$

Other matrixes are shown by

$$\begin{pmatrix} 0 \\ R_s \end{pmatrix} = \frac{1}{2\varepsilon_1 k_0} \begin{pmatrix} \varepsilon_1 k_0 + k_1 & \varepsilon_1 k_0 - k_1 \\ \varepsilon_1 k_0 - k_1 & \varepsilon_1 k_0 + k_1 \end{pmatrix} \begin{pmatrix} A_{s1} \\ B_{s1} \end{pmatrix} = M_{t1} \begin{pmatrix} A_{s1} \\ B_{s1} \end{pmatrix}, \tag{27a}$$

$$\begin{pmatrix} A_{sj} \\ B_{sj} \end{pmatrix} = \frac{1}{2\varepsilon_i k_j} \begin{pmatrix} (\varepsilon_i k_j + \varepsilon_j k_i)\exp(-ik_{sj}d_j) & (\varepsilon_i k_j - \varepsilon_j k_i)\exp(-ik_{sj}d_j) \\ (\varepsilon_i k_j - \varepsilon_j k_i)\exp(ik_{sj}d_j) & (\varepsilon_i k_j + \varepsilon_j k_i)\exp(ik_{sj}d_j) \end{pmatrix} \begin{pmatrix} A_{si} \\ B_{si} \end{pmatrix} = M_{ji} \begin{pmatrix} A_{si} \\ B_{si} \end{pmatrix}, \tag{27b}$$

and

$$\begin{pmatrix} A_{sj} \\ B_{sj} \end{pmatrix} = \frac{1}{2k_{sj}} \begin{pmatrix} (k_{sj} + \varepsilon_j k_{s0})\exp(-ik_{sj}d_j) & 0 \\ 0 & (k_{sj} - \varepsilon_j k_{s0})\exp(ik_{sj}d_j) \end{pmatrix} \begin{pmatrix} T_s \\ T_s \end{pmatrix} = M_{jb} \begin{pmatrix} T_s \\ T_s \end{pmatrix}, \tag{27c}$$

From these matrix relations, we find that the magnetic amplitudes of outputs R_s and T_s can be solved from the equations as follows:

$$\begin{pmatrix} 0 \\ R_s \end{pmatrix} = M_{t1}(M_{12}M_{21})^{N/2-1}M_{12} \left\{ M_{2a} \left[M_{a1}(M_{12}M_{21})^{N/2-1}M_{12}M_{2b} \begin{pmatrix} T_s \\ T_s \end{pmatrix} + \Gamma_2 \right] + \Gamma_1 \right\}, \tag{28a}$$

for the first structure,

$$\begin{pmatrix} 0 \\ R_s \end{pmatrix} = M_{t1}(M_{12}M_{21})^{(N-1)/2} \left\{ M_{1a} \left[M_{a2}(M_{21}M_{12})^{(N-1)/2}M_{2b} \begin{pmatrix} T_s \\ T_s \end{pmatrix} + \Gamma_2 \right] + \Gamma_1 \right\}, \tag{28b}$$

for the second, and

$$\begin{pmatrix} 0 \\ R_s \end{pmatrix} = M_{t1}(M_{12}M_{21})^{N/2-1}M_{12} \left\{ M_{2a} \left[M_{a2}(M_{21}M_{12})^{N/2}M_{21}M_{1b} \begin{pmatrix} T_s \\ T_s \end{pmatrix} + \Gamma_2 \right] + \Gamma_1 \right\}, \tag{28c}$$

for the last one. The output amplitudes cannot be found analytically, and numerical calculations must be done for them. In this work, we use the power densities of the input (incidence) and outputs to show the SHG, which are related to the amplitudes with

$$P_I = (\varepsilon_0/\mu_0)^{1/2}|I_0|^2/2, \tag{29a}$$

$$S_R = (\mu_0/\varepsilon_0)^{1/2}|R_s|^2/2, \tag{29b}$$

$$S_T = (\mu_0/\varepsilon_0)^{1/2}|T_s|^2/2, \tag{29c}$$

We see from the expressions of N_1, N_2, and N_3 that output amplitudes R_s and T_s are directly proportional to I_0^2 the square of electric amplitude of incidence wave. We conclude that the output densities are directly proportional to the square of the input (incident) density, or say the conversion efficiency $\alpha = S_{R,T}/P_I$ is directly proportional to the input density. For a fixed input density, if the SH outputs are intense, the conversion efficiency must be high. In the next section, we are going to compute numerically the output power densities.

III. NUMERICAL RESULTS AND DISCUSSIONS

In the vicinity of AF resonant frequencies, the nonlinear magnetic susceptibility is stronger, but the SH outputs also are controlled by the optical distances moved by them in the PC. We must carefully design the thicknesses of the AFF and dielectric layers to be favorable to the wave localization in the AFF and the transmission of the generated SH waves.

We take $N=9$ (N, the number of dielectric bilayer) for the structure with odd number of dielectric bilayers, and $N=8$ for others with even number of dielectric bilayers. Dielectric-1 layers are of SiO_2 with dielectric constant $\varepsilon_1 = 2.3$, and dielectric-2 layers are of ZnF_2 with $\varepsilon_2 = 8.0$. These dielectric layers are approximately considered as the half-wavelength films for the SH wave with frequency $\omega_s = 2\omega_2$. We use a MnF_2 film as the AFF in the structures. MnF_2 is a bisublattice uniaxial antiferromagnet in which the two sublattices possess the same ferromagnetic order, but are oppositely coupled with each other. Its net magnetization is vanished without any external magnetic field. Its physical parameters have been well known,[8,27] or the exchange field $H_e = 550$ kG, anisotropy field $H_a = 7.87$ kG, sublattice mag-

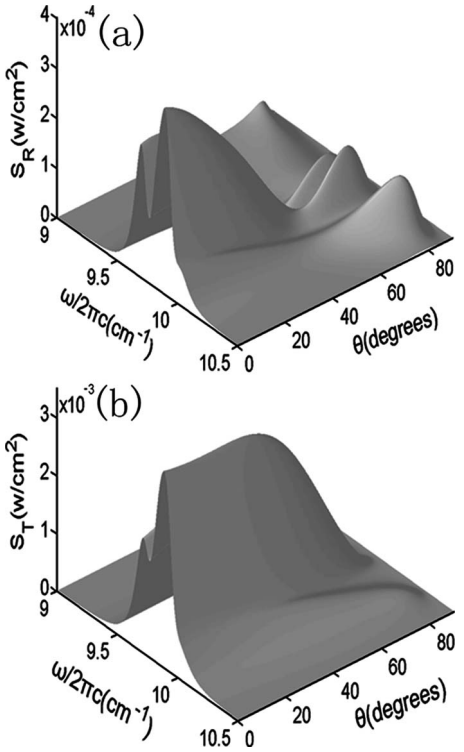

FIG. 2. SH output powers from a single AFF as the same as the AFF in the structures for the same incident power.

netization $M_0=0.6$ kG, gyromagnetic ratio $\gamma=1.97\times10^{10}$ rad s^{-1} kG^{-1}, and dielectric constant $\varepsilon_a=5.5$. The two resonant frequencies are $\omega_1/2\pi c=9.76$ cm^{-1} and $\omega_2/2\pi c=9.83$ cm^{-1} in the external magnetic field of $H_0=1.0$ kG. The AF damping coefficient is taken as $\tau=0.001$.

The layer thicknesses are fixed at $d_1=167$ μm, $d_2=89.6$ μm, and $d_a=255$ μm, except the situation where the layer-thickness dependence is discussed. The incident power density is fixed at $P_I=1.0$ kW/cm^2 much less than that in the previous papers,[1–4,6,7] but the same as that in reference 5. For comparison, the SH outputs of a single AFF are given in Fig. 2.[5]

We first discuss the SH outputs from the first structure (containing eight dielectric bilayers). In order to understand the SH outputs, the linear transmission spectra of the ω wave are shown in Fig. 3(a), where the top spectrum is for the structure without the AFF and the bottom is for that with the AFF. Due to the presence of the AFF, three defect modes are seen in the band gap and the band gap is modified, as shown in the bottom spectrum. The powers of SH outputs versus frequency and incident angle are illustrated in Figs. 3(b) and 3(c), respectively. It is very interesting that there are three obvious and narrow SHG bands of S_R or S_T and they correspond to the three defect modes, respectively. The middle band offers the most intense SH output. The highest output power and figure shapes are completely different from those for the single AFF (see Fig. 2). In order to explain these phenomena, an intensity distribution drawing of the ω wave

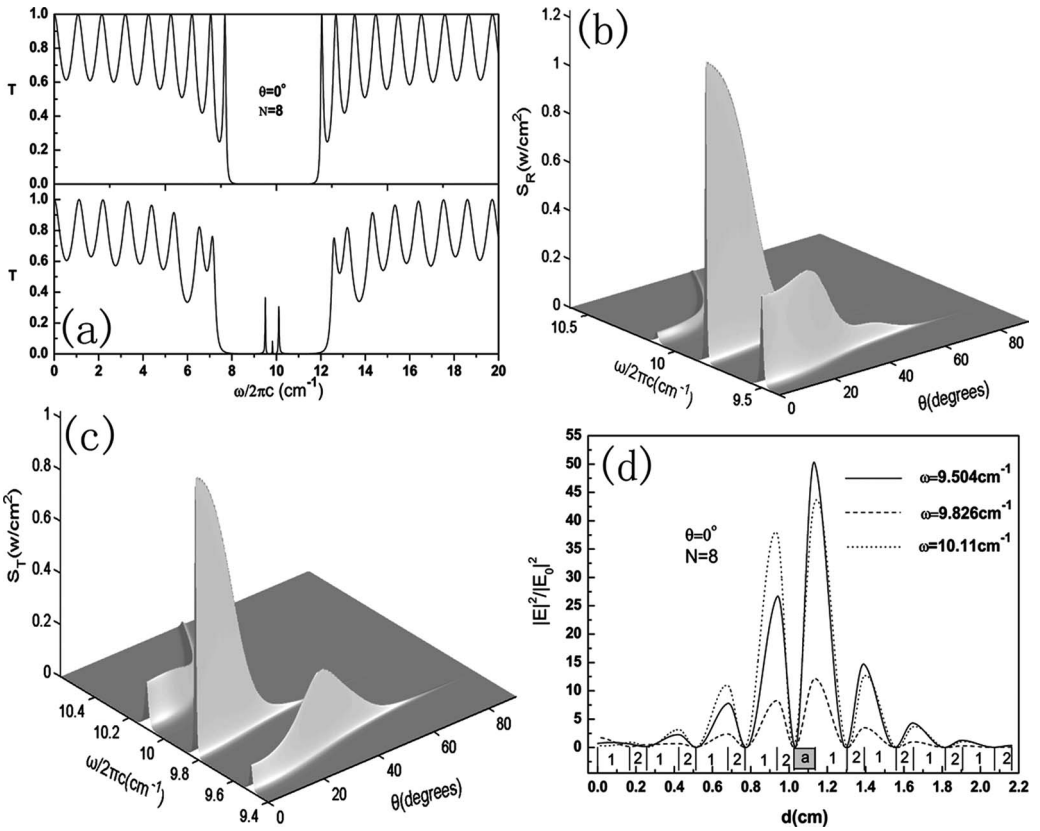

FIG. 3. Properties of the first structure: (a) the linear transmission spectra, (b) and (c) the SH output powers, and (d) the intensity distribution curves of the ω-waves related to the three bands.

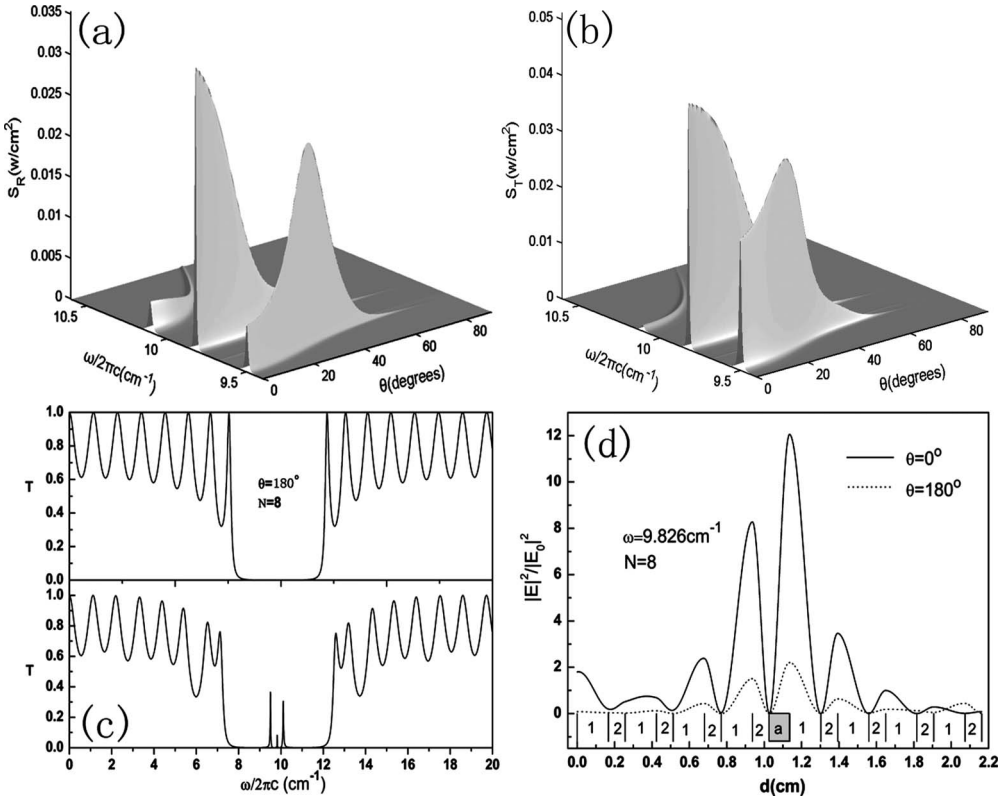

FIG. 4. In the case of reversed incident direction, the SH outputs are illustrated in (a) and (b), and the linear transmission spectra for the first structure without or with the AFF are shown in (c). In the two incident directions (θ=0 and π), the wave intensity distribution curves corresponding to the middle band are shown in (d).

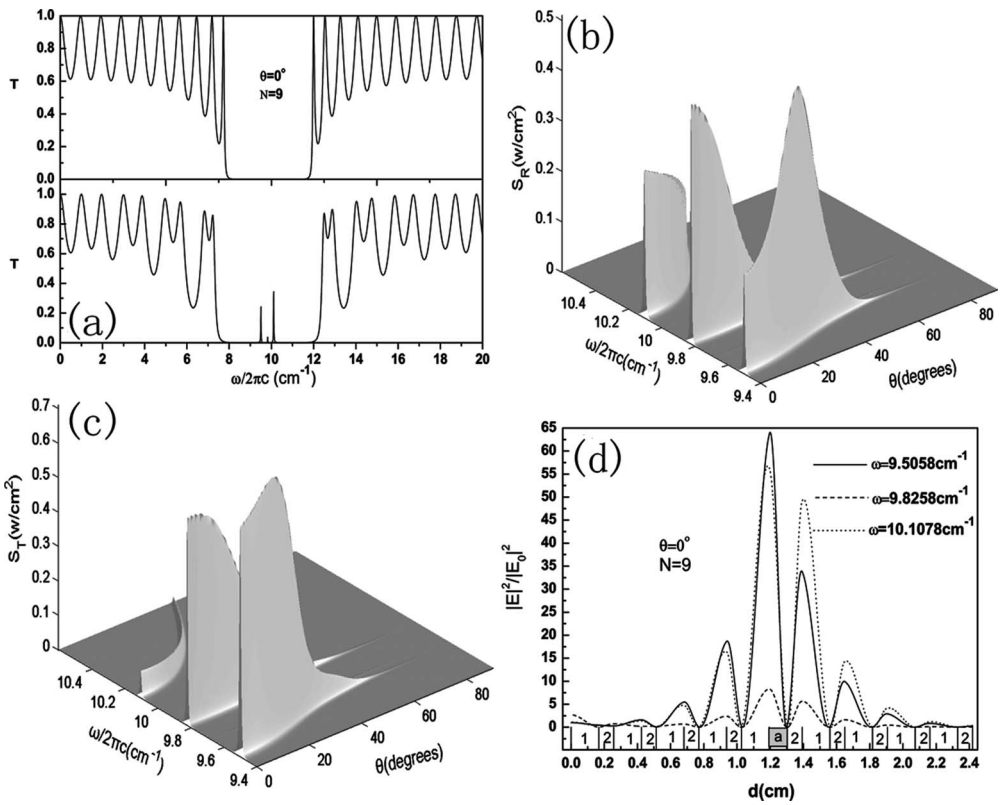

FIG. 5. Properties of the second structure: (a) the linear transmission spectra, (b) and (c) the SH output powers, and (d) the intensity distribution curves of the ω-waves related to the three bands.

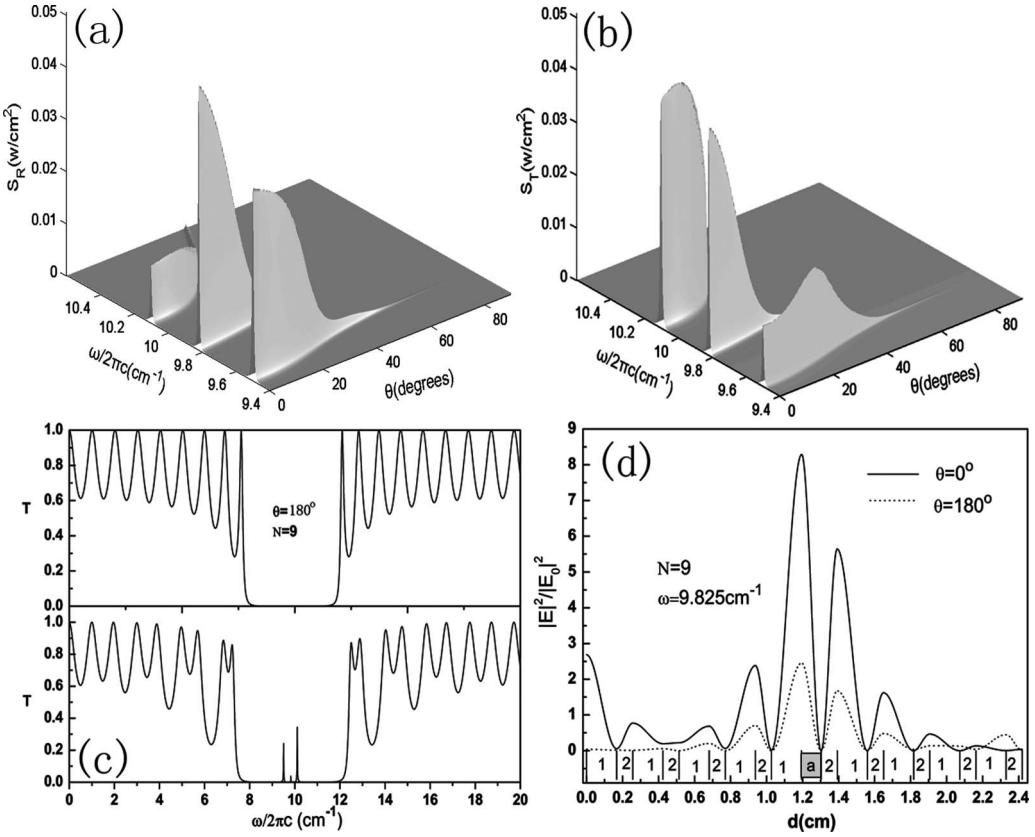

FIG. 6. In the case of reversed incident direction, the SH outputs are illustrated in (a) and (b), and the linear transmission spectra for the second structure without or with the AFF are shown in (c). In the two incident directions (θ=0 and π), the wave intensity distribution curves corresponding to the middle band are shown in (d).

in the structure is shown in Fig. 3(d) to explore the wave localization. The three curves correspond to the three SH output bands in the case of normal incidence, respectively. The middle band corresponds to the weakest localization and the highest pumping-wave intensity is about 12.5 times that of the incident wave. However, it is just situated at the resonant frequency ω_2=9.83 cm^{-1}, where the nonlinear magnetic susceptibility possesses a very large value so that this band offers the highest SH output, about S_R=1.2 W/cm^2. Although the other two bands are not situated at either of the resonant frequencies, their high localization (the highest pumping intensity is about 50 times that of the incident wave) still guarantees the intense SH outputs. Because of the filtering-wave effect of such a PC structure, the SH output bands are very narrow. Comparing the highest SH output power with that of the single AFF, the highest power is increased by about 350 times and is 20 times that in our previous work.[5] It should be mentioned that due to the thicknesses of dielectric layers designed according to ω_2, the highest SH output appears at ω_2, not at ω_1.

The first structure is an asymmetric system, so the SHG may be nonreciprocal. The nonreciprocity means that the SHG is different in intensity for the two incident waves of mutually opposite direction. Figs. 4(a) and 4(b) show the SH outputs in the opposite incident direction ($\theta+\pi$). Comparing these figures with Figs. 3(b) and 3(c), we find that the largest output power is decreased by about 27 times. The transmission spectra in Fig. 4(c) illustrate that the band gap and defect modes are not evidently changed by reversing the incident direction, but the localization effect is seriously decreased, as indicated in Fig. 4(d) in which the intensity distributions are given for the middle SH output band.

The second structure is different from the first structure. It contains odd number of dielectric bilayers (N=9) and the AFF is sandwiched between two dielectric layers of the fifth bilayer. The transmission spectra of the ω-wave are shown in Fig. 5(a), where the top spectrum is for the structure without the AFF and the bottom for the structure containing the AFF. Three defect modes appear in the band gap and the band gap also is modified by the presence of the AFF. Figs. 5(b) and 5(c) illustrate the SH outputs versus fundamental frequency and incident angle. Three obvious SHG bands also appear and correspond to the three defect modes. Comparing with those from the first structure, the SH output of the middle band is lowered, but those of the other two bands are heightened. The highest output comes from the low-frequency band of S_T and is situated at $\theta \approx 40°$. This output is smaller than that from the first structure. An intensity distribution drawing of the ω-wave is shown in Fig. 5(d), where the three curves correspond to the three SH output bands in the case of normal incidence, respectively. The wave localization related to the high- or low-frequency band is obviously stronger than that for the first structure, but that related to the middle band is weaker. It is evident that the localization effect causes the differences between the SH outputs in Figs. 3 and 5.

The second structure also is an asymmetric system, so the SHG is nonreciprocal. Figs. 6(a) and 6(b) show the SH out-

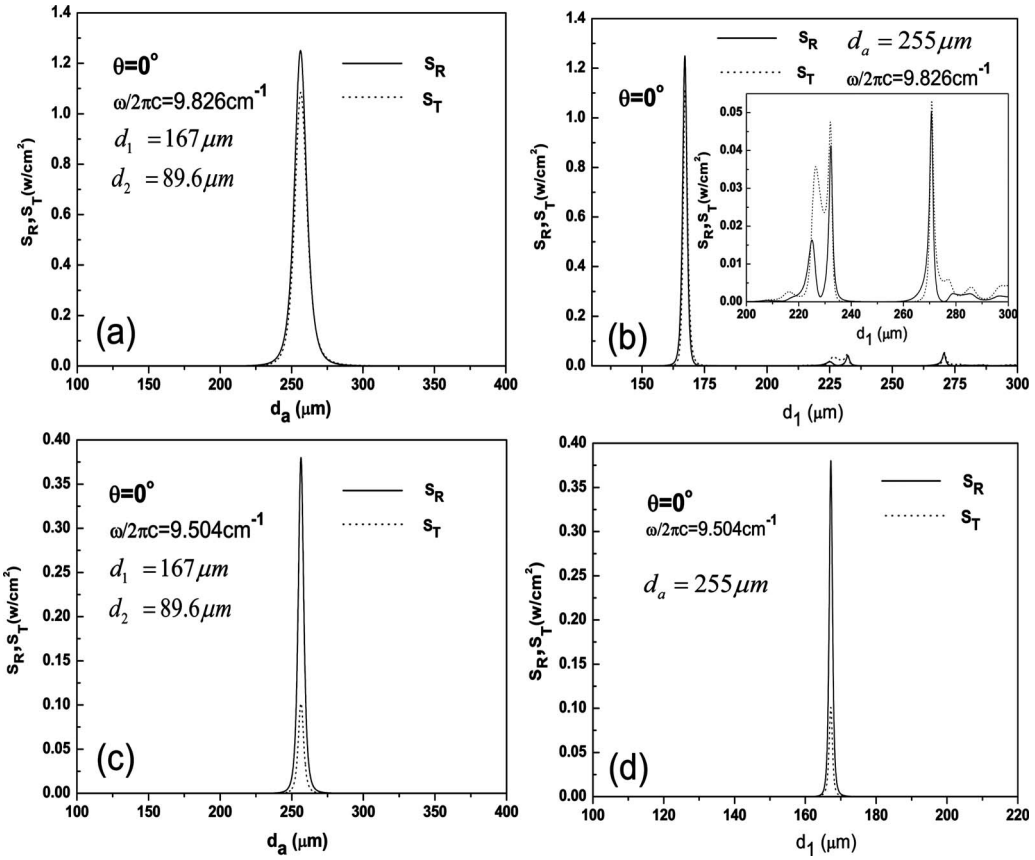

FIG. 7. Layer-thickness dependence of SHG for the two frequencies corresponding to the two SH output bands: (a) and (c) for the AFF thickness dependence at the fixed dielectric-layer thicknesses; (b) and (d) for the dielectric thickness dependence at the given AFF thickness. The two frequencies are indicated in the figures.

puts in the opposite incident direction. Comparing the two figures with Figs. 5(b) and 5(c), we find that the largest output power is decreased by about 12 times and the band shape is changed. Fig. 6(c) show that the band gap and defect modes also are not evidently influenced by reversing the incident direction, but the localization effect is serious decreased.

The last structure is of mirror-reflection symmetry with respect to the AFF. In this structure, there are eight dielectric bilayers. From the numerical results based on this structure, we are difficult to clearly see the defect modes related to the AFF. It is evident that the incident waves corresponding to the defect modes cannot effectively enter the AFF and most of their energy is reflected off. Thus the SH outputs are very weak, and the maximum is only $S_T \approx 6.0 \times 10^{-4}$ W/cm^2. This structure is the worst.

Finally, we examine the SH outputs versus AFF and dielectric-layer thicknesses. We take the first structure as an example since we find from the above discussions that it is the best for the SHG. Figure 7(a) illustrates the SH outputs as a function of AFF thickness for a frequency corresponding to the highest output band in Fig. 3(b) or Fig. 3(c). It is evident that there is the best value of AFF thickness, about 260 μm for the dielectric-layer parameters in this paper. The dielectric-layer thicknesses also influence seriously the SHG for a fixed AFF thickness. Fig. 7(b) shows the SH outputs versus d_1 for d_a=255 μm, with $d_2 = d_1\sqrt{\varepsilon_1/\varepsilon_2}$. The main peak corresponds to layer thickness d_1=167.5 μm (d_2 =89.8 μm) and the maximum SH output reaches about 1.3 W/cm^2. In the range between d_1=200 and 300 μm, there are some weak peaks, the corresponding SH outputs all are lower than 0.05 W/cm^2. For another frequency corresponding to the right output band in Fig. 3(b) or Fig. 3(c), we present Figs. 7(c) and 7(d) to show the layer-thickness dependence of the SHG. The best thicknesses still are d_a =260 μm, d_1=167 μm, and d_2=89.8 μm.

IV. SUMMARY

We have introduced another method to enhance the second harmonic generation (SHG) from an antiferromagnetic film (AFF). The AFF as the central layer is embedded in a one-dimensional photonic crystal composed of dielectric bilayers. The thicknesses of dielectric layers and the AFF are carefully designed in order to generate the high outputs of second harmonic waves. There are three typical structures with different symmetries. Besides the AFF, the first and third include even number of dielectric bilayers, but the second contains odd number of dielectric bilayers. For the SHG, we find that the best one is the first structure which contains even number of dielectric bilayers and is asymmetric. The highest SH output power reaches about 350 times that of a single AFF. The worst one is such a structure which also contain even number of dielectric bilayers, but is symmetric.

Opposite to the previous works,[3–5] here we find three obvious SHG bands and explain them with the wave localization effect and transmission spectra. The nonreciprocity of SHG is very obvious. If the incident wave irradiates the first and second structures in the direction opposite to the original direction, the SH output power can be changed by several dozen times. From the layer-thickness dependence of SH outputs, we found the best layer-thickness matching.

ACKNOWLEDGMENTS

This work was supported by the National Natural Science Foundation of China through Grant No. 10847112, and the Natural Science Foundation of Heilongjiang Province through Grant No. QC08C91.

APPENDIX

The derivation of SH magnetization and magnetic susceptibility will be done for an uniaxial AF in an external magnetic field $\vec{H}_0$. This AF contains two magnetic sublattices (SLs) which possess the same ferromagnetic structure and are oppositely coupled with each other, as shown in Fig. 8. We assume that the external magnetic field and AF anisotropy axis both are parallel to the z axis, so the static magnetization $\vec{M}_{0A}$ of SL A is parallel to the z axis and $\vec{M}_{0B}$ of SL B is antiparallel to the axis. The two magnetizations have the same amplitude M_0 in the case of no external magnetic field. In an additional alternating magnetic field $\vec{H}(\omega)$ considered as the first-order field, the total SL magnetizations obey the dynamic equations as

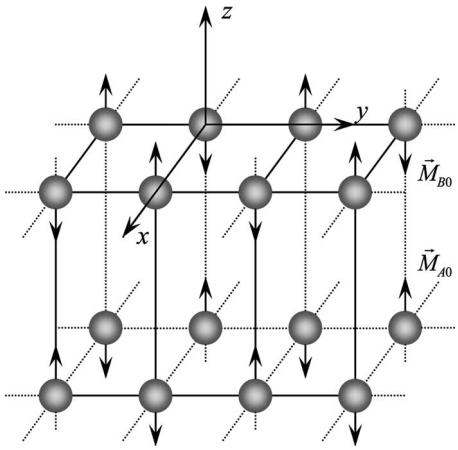

FIG. 8. The sketch of magnetic structure in an uniaxial anisotropic antiferromagnet and the coordinate system used in the Appendix.

$$\frac{\partial \vec{M}_l}{\partial t} = \gamma \vec{M}_l \times \vec{H}^l_{eff} + \frac{\tau}{M_0} \vec{M}_l \times \frac{\partial \vec{M}_l}{\partial t}, \tag{A1}$$

where γ and τ are the gyromagnetic ratio and damping. l is the SL index. The effective field on SL l is

$$\vec{H}^l_{eff} = \hat{e}_z(H_0 + H_a M_{lz}/M_0) - H_e \vec{M}_{l'}/M_0 + \vec{H}(\omega), \tag{A2}$$

where H_a and H_e are the anisotropy and exchange fields. Each SL magnetization contains two parts, or static and alternating parts, is written as $\vec{M}_l = \pm \hat{e}_z M_0 + \vec{m}_l$ with + for SL A and − for SL B. Thus Eq. (A1) can be decomposed into

$$\begin{aligned}\frac{\partial}{\partial t}\vec{M}_A = {} & \gamma\left\{ m_{Ay}\left[H_z + H_0 + H_a\frac{M_{Az}}{M_0} - H_e\frac{(-M_0+m_{Bz})}{M_0}\right] - (M_0+m_{Az})\left(-\frac{H_e}{M_0}m_{By}+H_y\right)\right\}\vec{e}_x + \gamma\left\{ -m_{Ax}\left[H_z + H_0 + H_a\frac{M_{Az}}{M_0}\right.\right. \\ & \left.\left. - H_e\frac{(-M_0+m_{Bz})}{M_0}\right] + (M_0+m_{Az})\left(-\frac{H_e}{M_0}m_{Bx}+H_x\right)\right\}\vec{e}_y + \gamma\left[m_{Ax}\left(-\frac{H_e}{M_0}m_{By}+H_y\right) - \left(-\frac{H_e}{M_0}m_{Bx}+H_x\right)m_{Ay}\right]\vec{e}_z \\ & + \frac{\tau}{M_0}\left\{\left[m_{Ay}\frac{\partial}{\partial t}m_{Az} - (M_0+m_{Az})\frac{\partial}{\partial t}m_{Ay}\right]\vec{e}_x + \left[(M_0+m_{Az})\frac{\partial}{\partial t}m_{Ax} - m_{Ax}\frac{\partial}{\partial t}m_{Az}\right]\vec{e}_y + \left[m_{Ax}\frac{\partial}{\partial t}m_{Ay} - m_{Ay}\frac{\partial}{\partial t}m_{Ax}\right]\vec{e}_z\right\},\end{aligned} \tag{A3a}$$

$$\begin{aligned}\frac{\partial}{\partial t}\vec{M}_B = {} & \gamma\left\{ m_{By}\left[H_z + H_0 + H_a\frac{M_{Bz}}{M_0} - H_e\frac{(M_0+m_{Az})}{M_0}\right] - (-M_0+m_{Bz})\left(-\frac{H_e}{M_0}m_{Ay}+H_y\right)\right\}\vec{e}_x + \gamma\left\{ -m_{Bx}\left[H_z + H_0 + H_a\frac{M_{Bz}}{M_0}\right.\right. \\ & \left.\left. - H_e\frac{(M_0+m_{Az})}{M_0}\right] + (-M_0+m_{Bz})\left(-\frac{H_e}{M_0}m_{Ax}+H_x\right)\right\}\vec{e}_y + \gamma\left[m_{Bx}\left(-\frac{H_e}{M_0}m_{Ay}+H_y\right) - \left(-\frac{H_e}{M_0}m_{Ax}+H_x\right)m_{By}\right]\vec{e}_z \\ & + \frac{\tau}{M_0}\left\{\left[m_{By}\frac{\partial}{\partial t}m_{Bz} - (-M_0+m_{Bz})\frac{\partial}{\partial t}m_{By}\right]\vec{e}_x + \left[(-M_0+m_{Bz})\frac{\partial}{\partial t}m_{Bx} - m_{Bx}\frac{\partial}{\partial t}m_{Bz}\right]\vec{e}_y + \left[m_{Bx}\frac{\partial}{\partial t}m_{By} - m_{By}\frac{\partial}{\partial t}m_{Bx}\right]\vec{e}_z\right\}.\end{aligned} \tag{A3b}$$

In the situation of the second-order approximation, $\vec{m}_l = \vec{m}_l^{(1)} + \vec{m}_l^{(2)}$.

Subsequently, we first determine the first-order magnetization and susceptibility. Neglecting the second-order terms in Eq. (A3) and considering that the linear SL magnetizations change with time according to $\exp(-i\omega t)$, Eq. (A3) are changed into

$$-i\omega\vec{m}_A = [(\omega_0 + \omega_a + \omega_e + i\tau\omega)m_{Ay}^{(1)} + \omega_e m_{By}^{(1)} - \omega_m H_y]\vec{e}_x - [(\omega_0 + \omega_a + \omega_e + i\tau\omega)m_{Ax}^{(1)} + \omega_e m_{Bx}^{(1)} - \omega_m H_x]\vec{e}_y, \tag{A4a}$$

$$-i\omega\vec{m}_B = [(\omega_0 - \omega_a - \omega_e - i\tau\omega)m_{By}^{(1)} - \omega_e m_{Ay}^{(1)} + \omega_m H_y]\vec{e}_x - [(\omega_0 - \omega_a - \omega_e - i\tau\omega)m_{Bx}^{(1)} - \omega_e m_{Ax}^{(1)} + \omega_m H_x]\vec{e}_y, \tag{A4b}$$

where the special frequencies are related to the fields by $\omega_0 = \gamma H_0$, $\omega_a = \gamma H_a$, and $\omega_e = \gamma H_e$, but $\omega_m = 4\pi\gamma M_0$. The AF alternating magnetization is defined as $\vec{m} = \vec{m}_A + \vec{m}_B$ but a supplementary definition $\vec{n} = \vec{m}_A - \vec{m}_B$ also will be used. According to $m_i^{(1)} = \Sigma_j \chi_{ij}^{(1)} H_j$ and $n_i^{(1)} = \Sigma_j N_{ij}^{(1)} H_j$, we find

$$\chi_{xx}^{(1)} = \chi_{yy}^{(1)} = \chi_1 = \omega_a'\omega_m\{1/[\omega_r'^2 - (\omega - \omega_0)^2] + 1/[\omega_r'^2 - (\omega + \omega_0)^2]\}, \tag{A5a}$$

$$\chi_{xy}^{(1)} = -\chi_{yx}^{(1)} = i\chi_2 = i\omega_a'\omega_m\{1/[\omega_r'^2 - (\omega - \omega_0)^2] - 1/[\omega_r'^2 - (\omega + \omega_0)^2]\}, \tag{A5b}$$

$$N_{xx}^{(1)} = N_{yy}^{(1)} = -2A\omega_0\omega_m Z_{-+}(\omega), \tag{A5c}$$

$$N_{xy}^{(1)} = -N_{yx}^{(1)} = 2iA\omega\omega_m Z_{+-}(\omega), \tag{A5d}$$

where $\omega_r'^2 = \omega_a'(2\omega_e + \omega_a')$ and $Z_{\pm\pm}(\omega) = \omega_r'^2 \pm \omega_0^2 \pm \omega^2$ with $\omega_a' = \omega_a + i\tau\omega$, but $A = \{[\omega_r'^2 - (\omega - \omega_0)^2][\omega_r'^2 - (\omega + \omega_0)^2]\}^{-1}$.

Finally we derive the SH magnetization and susceptibility based on the first-order magnetization. Reserving only the second-order terms changing with time according to $\exp(-2i\omega t)$ and noting $m_{lz}^{(1)} = 0$, we find from formulae (A3) that

$$-2i\omega\vec{m}_A^{(2)} = [\gamma m_{Ay}^{(1)} H_z + (\omega_0 + \omega_a + \omega_e + 2i\tau\omega)m_{Ay}^{(2)} + \omega_e m_{By}^{(2)}]\vec{e}_x + [-\gamma m_{Ax}^{(1)} H_z - (\omega_0 + \omega_a + \omega_e + 2i\omega\tau)m_{Ax}^{(2)} - \omega_e m_{Bx}^{(2)}]\vec{e}_y, \tag{A6a}$$

$$-2i\omega\vec{m}_B^{(2)} = [\gamma m_{By}^{(1)} H_z + (\omega_0 - \omega_a - \omega_e - 2i\omega\tau)m_{By}^{(2)} + \omega_e m_{Ay}^{(2)}]\vec{e}_x + [-\gamma m_{Bx}^{(1)} H_z - (\omega_0 - \omega_a - \omega_e - 2i\omega\tau)m_{Bx}^{(2)} + \omega_e m_{Ax}^{(2)}]\vec{e}_y. \tag{A6b}$$

Using $\vec{m}^{(2)} = \vec{m}_A^{(2)} + \vec{m}_B^{(2)}$ and $\vec{n}^{(2)} = \vec{m}_A^{(2)} - \vec{m}_B^{(2)}$, as well as $m_i^{(2)} = \Sigma_{jk}\chi_{ijk}^{(2)} H_j H_k$, from the x and y components of the SH magnetization, we find the corresponding nonzero elements

$$\chi_{xxz}^{(2)} = \chi_{xzx}^{(2)} = \chi_{xyz}^{(2)} = \chi_{xzy}^{(2)} = AB\frac{\omega_m^2\omega_0}{M_0}\{\omega_a' Z_{--}(\omega)Z_{-+}(2\omega) + \omega_a'' Z_{-+}(\omega)Z_{--}(2\omega) + 4\omega^2[\omega_a' Z_{+-}(2\omega) + \omega_a'' Z_{+-}(\omega)]\}, \tag{A7a}$$

$$\chi_{xyz}^{(2)} = \chi_{xzy}^{(2)} = -\chi_{yxz}^{(2)} = -\chi_{yzx}^{(2)} = -2AB\frac{i\omega\omega_m^2}{M_0}\{2\omega_0^2[\omega_a' Z_{-+}(2\omega) + 2\omega_a'' Z_{-+}(\omega)] + \omega_a'' Z_{+-}(\omega)Z_{--}(2\omega) + 2\omega_a' Z_{--}(\omega)Z_{+-}(2\omega)\}, \tag{A7b}$$

where $\omega_r''^2 = \omega_a''(\omega_a'' + 2\omega_e)$ and $Z_{\pm\pm}(2\omega) = \omega_r''^2 \pm \omega_0^2 \pm 4\omega^2$ with $\omega_a'' = \omega_a + 2i\omega\tau$, but $B = 1/[\omega_r''^2 - (2\omega + \omega_0)^2][\omega_r''^2 - (2\omega - \omega_0)^2]$.

The z components of sublattice SH magnetizations can be derived from

$$m_{Ax}^{(1)2} + m_{Ay}^{(1)2} + (M_0 + m_{Az}^{(2)})^2 = M_A^2, \tag{A8a}$$

$$m_{Bx}^{(1)2} + m_{By}^{(1)2} + (-M_0 + m_{Bz}^{(2)})^2 = M_B^2. \tag{A8b}$$

It is practical that the field $\vec{H}(\omega)$ is not very strong, so $M_l \approx M_0$. In this case, we obtain the formulae

$$m_{Az}^{(2)}(2\omega) = -\frac{1}{2M_0}[m_{Ax}^{(1)}(\omega)^2 + m_{Ay}^{(1)}(\omega)^2], \tag{A9a}$$

$$m_{Bz}^{(2)}(2\omega) = \frac{1}{2M_0}[m_{Bx}^{(1)}(\omega)^2 + m_{By}^{(1)}(\omega)^2], \tag{A9b}$$

which directly leads to

$$m_z^{(2)}(2\omega) = -\frac{1}{2M_0}[m_x^{(1)}n_x^{(1)} + m_y^{(1)}n_y^{(1)}]. \tag{A10}$$

Substituting the expressions of $m_i^{(1)}$ and $n_i^{(1)}$ into Eq. (A10), we obtain the rest nonzero elements of the SH magnetic susceptibility,

$$\chi_{zxx}^{(2)}(2\omega) = \chi_{zyy}^{(2)}(2\omega) = 2A\omega_m^2\omega_0\omega_a'/M_0. \tag{A11}$$

*Corresponding author; xzwang696@126.com

[1] N. S. Almeida and D. L. Mills, Phys. Rev. B **36**, 2015 (1987).
[2] L. Kahn, N. S. Almeida, and D. L. Mills, Phys. Rev. B **37**, 8072 (1988).
[3] S.-C. Lim, J. Opt. Soc. Am. B **19**, 1401 (2002).
[4] S.-C. Lim, J. Phys.: Condens. Matter **18**, 4329 (2006).
[5] S. Zhou and X.-Z. Wang, J. Opt. Soc. Am. B **25**, 1639 (2008).
[6] J. Bai, S. Zhou, F.-L. Liu, and X.-Z. Wang, J. Phys.: Condens. Matter **19**, 046217 (2007).
[7] Xuan-Zhang Wang and Hua Li, Phys. Rev. B **72**, 054403 (2005).
[8] K. Abraha and D. R. Tilley, Surf. Sci. Rep. **24**, 129 (1996).
[9] U. K. Sapaev, I. A. Kulagin, and T. Usmanov, J. Opt. B: Quantum Semiclassical Opt. **5**, 355 (2003).
[10] A. A. Rzhevsky, B. B. Krichevtsov, D. E. Bürgler, and C. M.

Schneider, Phys. Rev. B **75**, 144416 (2007).
[11] M. Fiebig, D. Frohlich, B. B. Krichevtsov, and R. V. Pisarev, Phys. Rev. Lett. **73**, 2127 (1994).
[12] M. Fiebig, D. Frohlich, T. Lottermoser, R. V. Pisarev, and H. J. Weber, Phys. Rev. Lett. **87**, 137202 (2001).
[13] M. Fiebig, V. V. Pavlov, and R. V. Pisarev, J. Opt. Soc. Am. B **22**, 96 (2005).
[14] E. Yablonovitch and T. J. Gmitter, Phys. Rev. Lett. **63**, 1950 (1989).
[15] J. D. Joannopoulos, P. R. Villeneuve, and S. Fan, Nature (London) **386**, 143 (1997).
[16] G. Parker and M. Charlton, Phys. World **8**(11), 29 (2000).
[17] F.-F. Ren, Li Rui, Cheng Chen, H.-T. Wang, J. Qiu, J. Si, and K. Hirao, Phys. Rev. B **70**, 245109 (2004).
[18] B Shi, Z. M. Jiang, and Xun Wang, Opt. Lett. **26**, 1194 (2001).
[19] Q. Zhu, D. Wang, and Y. Zhang, J. Opt. A, Pure Appl. Opt. **10**, 025201 (2008).
[20] F. Wang, S. N. Zhu, K. F. Li, and K. W. Cheah, Appl. Phys. Lett. **88**, 071102 (2006).
[21] I. L. Lyubchanskii, N. N. Dadoenkova, M. I. Lyubchanskii, E. A. Shapovalov, and Th. Rasing, J. Phys. D **36**, R277 (2003).
[22] M. Inoue, R. Fujikawa, and A. Baryshev, A. Khanikaev, P. B. Lim, H. Uchida, O. Aktsipetrov, A. Fedyanin, T. Murzina, and A. Granovsky, J. Phys. D **39**, R151 (2006).
[23] I. L. Lyubchanskii, N. N. Dadoenkova, A. E. Zabolotin, Y. P. Lee, and Th. Rasing, J. Appl. Phys. **103**, 07B321 (2008).
[24] A. Figotin and I. Vitebsky, Phys. Rev. E **63**, 066609 (2001).
[25] M. Inoue and T. Fujii, J. Appl. Phys. **81**, 5659 (1997).
[26] Xuan-Zhang Wang, J. Phys.: Condens. Matter **17**, 5447 (2005).
[27] N. S. Almeida and D. L. Mills, Phys. Rev. B **37**, 3400 (1988).